

ADAPTING BIOLOGICAL REFLEXES FOR DYNAMIC REORIENTATION IN SPACE MANIPULATOR SYSTEMS

Daegyun Choi^{*}, Alhim Vera[†], and Donghoon Kim[‡]

Robotic arms mounted on spacecraft, known as space manipulator systems (SMSs), are critical for enabling on-orbit assembly, satellite servicing, and debris removal. However, controlling these systems in microgravity remains a significant challenge due to the dynamic coupling between the manipulator and the spacecraft base. This study explores the potential of using biological inspiration to address this issue, focusing on animals, particularly lizards, that exhibit mid-air righting reflexes. Based on similarities between SMSs and these animals in terms of behavior, morphology, and environment, their air-righting motion trajectories are extracted from high-speed video recordings using computer vision techniques. These trajectories are analyzed within a multi-objective optimization framework to identify the key behavioral goals and assess their relative importance. The resulting motion profiles are then applied as reference trajectories for SMS control, with baseline controllers used to track them. The findings provide a step toward translating evolved animal behaviors into interpretable, adaptive control strategies for space robotics, with implications for improving maneuverability and robustness in future missions.

INTRODUCTION

Background

Space manipulator systems (SMSs), composed of spacecraft equipped with robotic arms, are essential for enabling in-space servicing, assembly, and manufacturing, as well as debris removal. Remarkable examples of SMSs that have demonstrated their capabilities in space include the Engineering test satellite no. 7 (ETS-VII), developed by the National Space Development Agency of Japan¹ and autonomous space transport robotic operations (ASTRO) system, developed by Boeing Integrated Defense Systems.² The successful demonstrations of both SMSs have shown the viability of autonomous robotic operations in orbit. These missions highlight the increasing need for high-precision, energy-efficient, and adaptable manipulation strategies to support the growing complexity of future space missions.

In microgravity, SMSs face unique challenges despite considerable progress in operating and testing them on orbit. Unlike terrestrial manipulators anchored to rigid bases, robotic arms in space

^{*}Postdoctoral Researcher, Department of Aerospace Engineering & Engineering Mechanics, University of Cincinnati, Cincinnati, OH 45221, USA.

[†]Graduate Student, Department of Aerospace Engineering & Engineering Mechanics, University of Cincinnati, Cincinnati, OH 45221, USA.

[‡]Assistant Professor, Department of Aerospace Engineering & Engineering Mechanics, University of Cincinnati, Cincinnati, OH 45221, USA.

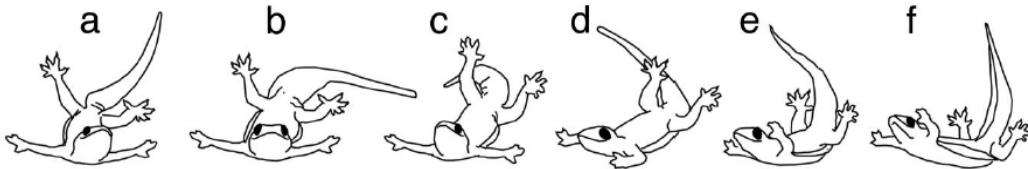


Figure 1: Sequence of Aerial Righting of Gecko. Adapted from¹¹ Copyright (2008) National Academy of Sciences.

operate from a floating spacecraft. This introduces strong dynamic coupling—any motion of the arm(s) induces a reactive motion on the base spacecraft, affecting overall system stability and control accuracy.³ Additionally, constraints on fuel, computational power, and safety require appropriate motion planning strategies that can execute with high efficiency and reliability.

Traditional optimal control techniques have focused on minimizing relative distances to targets⁴ or reducing energy consumption,⁵ while considering several factors, such as collision avoidance, singularity avoidance, and the robotic arm’s limited capabilities. However, these methods are computationally expensive and can be difficult to implement in real-time operations. Furthermore, they may lack robustness under uncertainties in real-world space environments. On the other hand, some researchers have studied reinforcement learning and other artificial intelligence-based techniques for SMS control to overcome the traditional methods’ drawbacks.⁶ Such approaches offer a more adaptive solution space and greater robustness against uncertainties.⁷ However, their black-box nature and lack of interpretability, making it difficult for control engineers to understand their decision-making, present challenges for implementation in high-assurance and safety-critical space robotic systems.⁸

Problem Statement

To overcome these limitations, this research investigates a biologically inspired operational strategy that leverages optimization principles observed in nature. Animals, such as cats, squirrels, and especially geckos, have evolved mid-air righting reflexes that achieve stability, efficiency, and safety under dynamic conditions. For example, cats dynamically twist their bodies to right themselves and land safely during unexpected falls,⁹ and squirrels utilize their tails to stabilize their posture during free-fall situations.¹⁰ In addition, as shown in Figure 1, lizards reorient in mid-air by swinging their tails to redistribute angular momentum,^{11,12} a mechanism that parallels momentum exchange in SMSs. These strategies result from natural optimization processes that balance various objectives, such as stability, agility, and energy conservation.

This work hypothesizes that evolved animal behaviors can inform the design of interpretable and robust control strategies for SMSs in microgravity. To validate this hypothesis, the research focuses on biomechanical modeling of lizard motion and the extraction of tail-body coordination patterns using computer vision techniques. The extracted trajectories are then used to identify multiple objectives and their corresponding weighting factors, providing a mathematical interpretation of the animals’ evolved behaviors. These motion trajectories serve as reference inputs to a dynamic model of an SMS, enabling evaluation of its behavior and comparison with animal motion. These insights lay the groundwork for developing adaptive and efficient control strategies for future autonomous SMS operations.

PROPOSED METHODOLOGY AND RESULTS

The proposed methodology aims not only to understand the animals' evolved behaviors by identifying similarities with SMSs and extracting motion trajectories, but also to implement these trajectories into the SMS dynamics model as reference inputs. These reference trajectories guide the controller in generating appropriate control inputs while allowing for the analysis of the underlying behavioral objectives.

The overall process consists of three main steps:

Step 1: Identification of Similarities and Objective Formulation The first step involves identifying behavioral, morphological, and environmental similarities between biological systems and SMSs. Motivated by the widely supported view that evolved animal behaviors embody natural optimization principles, an objective function containing multiple objectives and weighting factors is formulated. This study focuses on a single robotic arm-mounted spacecraft configuration, modeled after real-world missions, such as ETS-VII and ASTRO. Building on these comparisons, the righting reflex observed in lizards is chosen for deeper investigation.

Step 2: Motion Trajectory Extraction via Computer Vision To model animals' righting reflexes, motion trajectories are extracted from recorded videos of lizards in free-fall using various computer vision techniques. Key body segments involved in mid-air reorientation are identified through this analysis, enabling the construction of a biomechanical model of the observed behavior.

Step 3: Integration and Control Evaluation in SMS (In progress) The extracted trajectories and identified body segment dynamics are then used to infer the objectives and weighting factors within the previously defined optimization framework, focusing on metrics, such as safety, stabilization, and efficiency. These trajectories are implemented as reference paths in the SMS dynamics model. Controllers, such as proportional-integral-derivative, linear-quadratic regulator, or model predictive control, are planned for this task. By observing the SMS's behavior under these control schemes, the influence of different weighting factors in the objective function can be evaluated and analyzed.

Identification of Similarities and Objective Formulation

Behavioral Similarities In nature, animal motion reflects evolved strategies for surviving in dynamic and uncertain environments, often balancing competing objectives, such as stability, agility, and energy efficiency.^{13,14} During free-fall scenarios (Figure 1), lizards exhibit active body adjustments that reflect these priorities. Such behaviors can be interpreted as solutions to a multi-objective optimization problem influenced by environmental constraints and internal priorities:¹⁵

$$\min J = w_1\phi_{\text{safety}} + w_2\phi_{\text{stability}} + w_3\phi_{\text{efficiency}}. \quad (1)$$

Here, w_i represent the weighting coefficients for each behavioral component, ϕ_{safety} reflects critical survival actions (e.g., protecting the head), $\phi_{\text{stability}}$ reflects postural control or reorientation, and $\phi_{\text{efficiency}}$ penalizes unnecessary energy expenditure. These weights shift dynamically depending on task demands or environmental stimuli.

Similarly, SMS operations can be formulated as a multi-objective optimization problem, where performance metrics like collision avoidance, energy usage, and disturbance minimization must be balanced under dynamic coupling and physical constraints. Like animals, SMSs must adapt to disturbances while maintaining task success. The behavioral analogies between animals and SMSs are summarized in Table 1.

Table 1: Behavioral Analogy

Aspect	Lizards	SMSs	Analogy
Safety	Instinctively reorient during a fall using tail and limbs to reduce impact risk	Uses onboard attitude control (e.g., thrusters, reaction wheels) to correct orientation during unexpected motion	Both respond rapidly to restore a safe orientation when destabilized
Stabilization	Adjust body posture mid-air through coordinated limb and tail movement	Coordinates base and arm movements to maintain or regain system stability	Both rely on internal coordination to stabilize themselves during motion
Efficiency	Executes reorientation with minimal, well-timed effort	Employs optimized control laws to correct attitude with minimal energy use	Both achieve orientation correction without excessive energy expenditure

While certain behavioral analogies exist between lizards and SMSs, notable differences remain, particularly in environmental context and movement timescales. SMSs typically perform slow, deliberate motions over extended durations during proximity operations, whereas lizards execute righting reflexes in free-fall conditions that last less than one second and involve significant vertical displacement.¹¹ Although aerodynamic drag may play a role in lizard reorientation, it is considered negligible here due to the short duration of the fall, the small effective surface area, and the lack of fur, unlike animals, such as cats or squirrels.

As shown in Figure 1, lizards use rapid tail motions to reorient themselves mid-air, movements far quicker than those achievable by current SMS actuation systems. To bridge this gap, the planned work involves scaling and modifying the extracted lizard motion trajectories to fit within the physical and dynamic constraints of SMS. This approach enables a practical transfer of biologically inspired strategies to robotic systems operating in space.

Morphological Similarity This work mainly concentrates on an SMS configuration featuring a single robotic arm, such as those found in ETS-VII and ASTRO. Among various animals known for their righting reflexes, lizards present a particularly strong geometric analogy to actual SMS platforms. To examine this morphological similarity, one compares the segment proportions between lizards and SMSs. As shown in Table 2, the relative segment lengths exhibit notable alignment. For instance, a lizard’s tail accounts for approximately 57% of its total body length, which is comparable to the reach of a robotic arm relative to one side of the spacecraft base. This geometric similarity supports the suitability of lizards as a biological analog for analyzing SMS behavior.

Figure 2 further illustrates this relationship: the body (in orange) and tail (in blue) segmentation in lizards is directly compared with two satellite-manipulator systems. In both biological and engineered systems, the elongated appendage (tail or robotic arm) can serve as an actuator for body reorientation and interaction with the environment.

However, in terms of mass, although the mass ratio of the robotic arm in SMSs differs from that of lizards, this ratio does not account for the payload mass in SMSs. This available margin for additional mass on the robotic arm allows us to explore various payloads during SMS operation in the analysis.

Table 2: Morphological Analogy

Aspect	Lizards ¹⁶	SMSs ^{1,2}	Analogy
Primary body segments	2 (body & tail) 0.31 – 0.65	2 (spacecraft & robotic arm) 0.35 – 0.43	Shown in Figure 2
Length ratio (tail or arm / total length)	~ 0.2	≥ 0.05	Comparable segment proportions
Mass ratio (tail or arm / body or base mass)	$\sim \infty$	≥ 0.05	Can be comparable when accounting for SMS payload mass
Degree of freedom (DOF)	$\sim \infty$	12 (6 + 6)	Depends on the motion of interest in lizards
Detailed body segments	$\sim \infty$	7 (1 + 6)	Approximation depends on modeling objectives

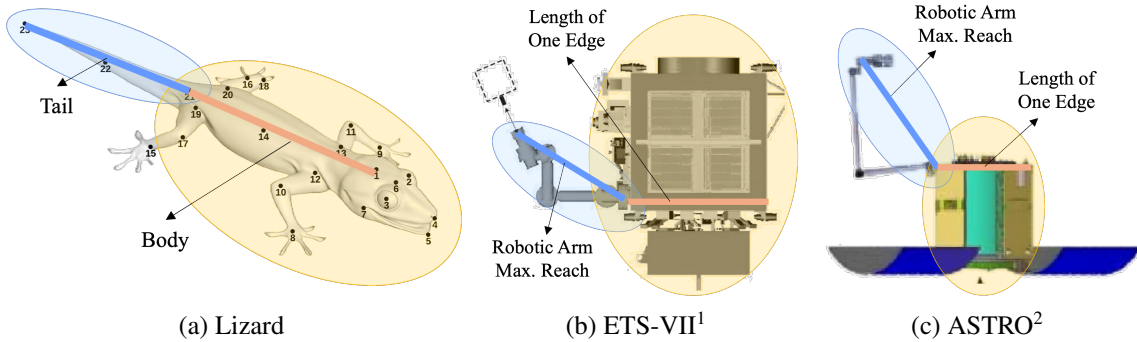


Figure 2: Visual Comparison of Lizard and SMSs

From a modeling perspective, both lizards and SMSs can be treated as multi-body systems with jointed segments. Their dynamics are governed by the standard equations of motion:¹⁷

$$M(\mathbf{q})\ddot{\mathbf{q}} + C(\mathbf{q}, \dot{\mathbf{q}})\dot{\mathbf{q}} + \mathbf{g}(\mathbf{q}) = \boldsymbol{\tau} + \boldsymbol{\tau}_d, \quad (2)$$

where $M \in \mathbb{R}^{m \times m}$ is the mass/inertia matrix, $C \in \mathbb{R}^{m \times m}$ is the Coriolis and centrifugal matrix, $\mathbf{g} \in \mathbb{R}^m$ is a vector related to the gravity term, $\mathbf{q} \in \mathbb{R}^m$ represents the joint configuration, $\boldsymbol{\tau} \in \mathbb{R}^m$ denotes the applied joint torques, and $\boldsymbol{\tau}_d \in \mathbb{R}^m$ indicates the disturbances, like air drag, acting on the system. Note that the gravity term is generally assumed to be zero for SMSs. When external force and torque acting on the system are zero, the system exhibits momentum conservation, a key principle underlying both lizard mid-air motion and SMS motion. This property implies that movement in one segment, such as a lizard's tail, induces reactive motion in another, like the torso, mirroring how the motion of an SMS's robotic arm perturbs the spacecraft base. In fact, the number of DOF and detailed body segments differs because lizards have a flexible body. However, these can be appropriately modeled depending on the specific motion of interest, which will be discussed in Step 2.

Environmental Similarity Even though lizards experience less aerodynamic drag in mid-air, gravity can still introduce behavioral discrepancies. This work mainly considers free-fall conditions for observing lizards' behavior, as these conditions closely resemble the microgravity environments in which SMSs operate. In fact, empirical studies^{18,19} support using free-fall settings to examine

Table 3: Environmental Analogy

Aspect	Lizards	SMSs	Analogy
Air drag effect	Present, but minimal due to small size and rapid falling	Dependent on orbit, but typically negligible	Both experience negligible air drag
Gravity effect*	Microgravity during free fall conditions	Microgravity	Both experience microgravity

* Some studies^{18,19} show that lizards' self-righting behavior in space is similar to that on Earth.

lizards' righting reflex behavior.

These studies show that geckos exhibit skydiving-like limb extensions and tail actuation during free-fall in space, closely mimicking their terrestrial mid-air responses. This reinforces the hypothesis that mid-air animal behaviors, optimized for gravity-dominated environments, remain valid in microgravity or near-zero-g contexts. Despite differences in mass, air drag, and actuation dynamics, this environmental similarity, along with behavioral and morphological parallels, suggests that biologically inspired movement primitives can inform SMS operation strategies.

These observations form the theoretical basis for this work: translating righting reflexes observed in lizards into operational strategies for SMSs. By extracting motion patterns from animal data and understanding their governing dynamics, the goal is to build a foundation for interpretable and adaptive SMS control frameworks based on biological intelligence.

Motion Trajectory Extraction via Computer Vision

To efficiently obtain, evaluate, and analyze the motion data, this study constructs a computer vision-based pipeline focused on extracting the lizard's motion trajectories. The structured pipeline for motion pattern extraction, developed in the authors' previous work,²⁰ consists of five steps: i) Segmentation is performed using the segment anything model²¹ to focus on the object of interest in the video frames; ii) Pose estimation is conducted with ViTPose++²² to estimate the pose information of the object based on keypoints around it; iii) Tracking is handled by CoTracker²³ to continuously track the detected keypoints; iv) Temporal smoothing and identity re-association are implemented using a centroid-based optimization strategy, ensuring reliable multi-frame trajectories for analysis; v) Transformation from 2-dimensional (2D) image coordinates to 3D world coordinates is conducted to reconstruct the 3D information and compute the motion trajectories.

Body Segment Identification To obtain effective motion trajectories that describe righting reflexes, this work begins by identifying the segments and keypoints of lizard anatomy. The anatomical structure is extracted from the Animal Kingdom dataset. As shown in Figure 3, each of the 23 keypoints corresponds to a distinct anatomical location critical for dynamic modeling. With these keypoints, motions across approximately 14 body segments can be observed.

To evaluate the feasibility of motion trajectory extraction, each individual keypoint is identified from real free-fall high-speed video recordings of a lizard,²⁴ as shown in Figure 4. Each extracted keypoint is then analyzed in terms of its movement and visibility, as presented in Table 4. Due to resource constraints, only a limited number of videos are processed; however, additional data will be collected to improve statistical confidence. The movement analysis quantifies the frame-to-frame displacement of each keypoint using Euclidean distance in pixel space.

The average movement for each point is computed across all frames, and visibility is calculated

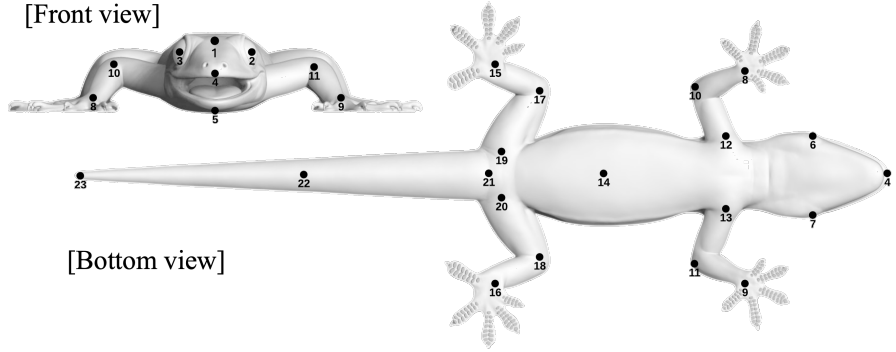


Figure 3: Annotated 23 Keypoints in Lizard and 14 Anatomical Body Segments

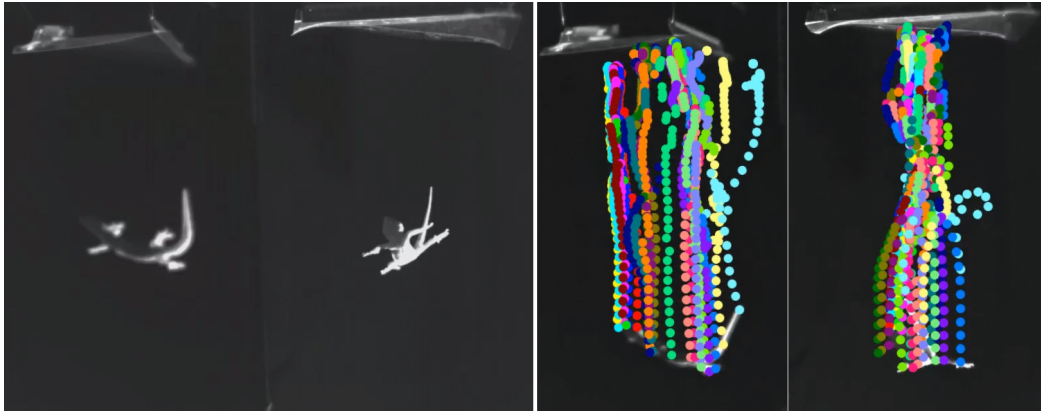


Figure 4: Capture of the Original Video²⁴ (left) and the Keypoints Extraction (right)

as the percentage of frames in which the point is successfully tracked. To facilitate comparative analysis across different anatomical regions, movements are normalized relative to the maximum observed movement across all points.

Notably, points along the tail (21–23), hips (19–20), and knees (17–18) show high movement and visibility, highlighting their role in dynamic body reorientation. In contrast, points near the mouth (4–7) and eye (2–3) show low movement and frequent occlusion, making them less useful for reliable modeling.

To evaluate the temporal reliability of keypoints during dynamic motion, a stability analysis based on frame-wise time series data is performed. This analysis helps determine which anatomical landmarks remain consistently trackable, which drift erratically, and which are frequently lost due to occlusion. These insights are essential for obtaining continuous trajectory information.

Table 5 summarizes several key metrics used to assess the tracking stability of each point:

- Max gap length – The longest sequence of consecutive frames during which the point was not detected. Smaller gaps indicate better continuity.
- Position variance – The statistical variance in the keypoint’s position, providing a raw measure of how much its location changes over time.
- Drift score – A normalized indicator of erratic movement; lower values signify that the keypoint remains stable in space.

Table 4: Average Movement and Visibility of Keypoints

Keypoints	Point name	Average movement (pixel)	Visibility (%)
1	Neck	0.53	22.10
2	Eye_Left	0.24	13.20
3	Eye_Right	0.44	18.40
4	Mouth_Front_Top	0.24	16.20
5	Mouth_Front_Bottom	0.72	14.70
6	Mouth_Back_Right	0.65	19.90
7	Mouth_Back_Left	0.35	19.10
8	Wrist_Right	0.53	22.10
9	Wrist_Left	1.86	25.00
10	Elbow_Right	1.22	24.30
11	Elbow_Left	0.51	22.10
12	Shoulder_Right	1.33	22.80
13	Shoulder_Left	0.50	22.10
14	Torso_Mid_Back	0.79	14.00
15	Ankle_Right	1.41	23.50
16	Ankle_Left	1.80	33.80
17	Knee_Right	1.38	30.10
18	Knee_Left	2.12	27.90
19	Hip_Right	0.95	27.90
20	Hip_Left	4.35	30.10
21	Tail_Top_Back	0.66	22.10
22	Tail_Mid_Back	0.96	13.20
23	Tail_End_Back	2.67	18.40

- Stability category – A high-level classification based on the combination of all metrics, categorizing each point as *Stable*, *Moderately Stable*, *Drifting*, *Frequently Occluded*, or *Occluded*.

The stability analysis revealed that most keypoints suffered from frequent occlusion or drift during the observed free-fall sequences. As shown in Table 5, all points were ultimately categorized as *Occluded*, highlighting the challenges of reliable tracking under dynamic conditions. Despite this, certain keypoints, such as 19, 21, and 23, exhibited comparatively lower drift scores and moderate visibility, suggesting partial robustness.

Of particular interest for control strategies in SMSs are points with low drift scores (e.g., keypoint 21 at 0.01 and keypoint 19 at 0.12), which may serve as inertial references or anchors in future reconstruction frameworks. However, the prevalence of long occlusion gaps (up to 60 consecutive frames) and limited visibility across the board emphasizes the need for either improved multi-camera coverage or refined prediction models to enhance reliability.

Based on this comprehensive evaluation, which includes movement magnitude, visibility, temporal continuity, and drift behavior, a reduced set of 11–17 keypoints is selected, excluding those around the eyes and mouth. These keypoints are grouped into *six primary segments*: the *body*, *tail*, and *four legs*, as highlighted in blue in Figure 5.

This selection prioritizes keypoints that are both biomechanically relevant and statistically stable across frames, ensuring robustness against occlusion and erratic motion. Note that each body seg-

Table 5: Keypoints Tracking Stability Metrics Across Free-Fall Sequences (Total: 140 frames)

Keypoints	Point name	Max gap length (frame)	Drift score (0/1)	Position variance	Stability category
1	Neck	60	1.00	9.50	occluded
2	Eye_Left	59	0.50	0.16	occluded
3	Eye_Right	54	0.51	1.27	occluded
4	Mouth_Front_Top	56	0.06	0.14	occluded
5	Mouth_Front_Bottom	60	0.33	5.63	occluded
6	Mouth_Back_Right	56	0.52	10.69	occluded
7	Mouth_Back_Left	60	0.11	2.07	occluded
8	Wrist_Right	60	0.47	9.62	occluded
9	Wrist_Left	51	1.00	27.35	occluded
10	Elbow_Right	46	0.79	26.68	occluded
11	Elbow_Left	60	0.24	11.74	occluded
12	Shoulder_Right	47	0.63	22.95	occluded
13	Shoulder_Left	60	0.24	11.88	occluded
14	Torso_Mid_Back	60	0.16	7.74	occluded
15	Ankle_Right	60	0.50	65.20	occluded
16	Ankle_Left	45	0.68	45.92	occluded
17	Knee_Right	46	0.63	40.96	occluded
18	Knee_Left	52	0.54	121.34	occluded
19	Hip_Right	52	0.12	19.44	occluded
20	Hip_Left	52	0.55	639.61	occluded
21	Tail_Top_Back	60	0.01	16.92	occluded
22	Tail_Mid_Back	60	0.21	9.86	occluded
23	Tail_End_Back	60	0.15	189.43	occluded

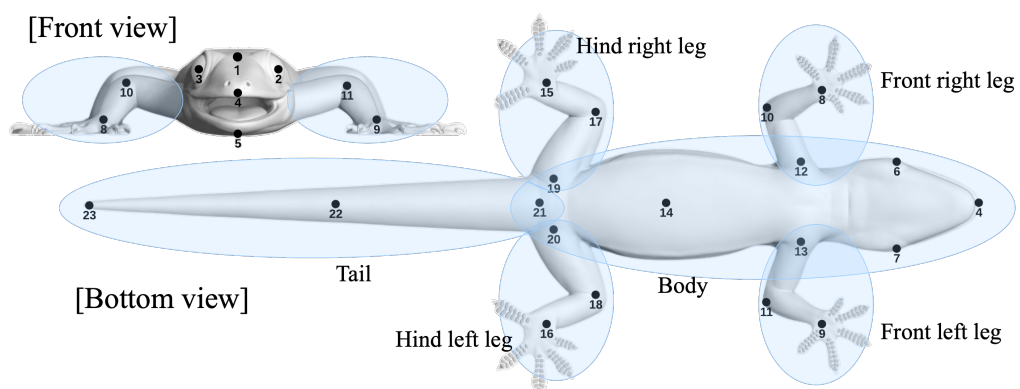


Figure 5: Selected 6 Primary Anatomical Body Segments

ment, such as the body, tail, and four legs, can be represented as the robotic arm, base spacecraft, and actuators, respectively. Although the legs display relatively small movements during self-righting, their influence on the body's motion trajectory warrants further analysis in conjunction with Step 3 to refine the biomechanical model. The proposed configuration balances model simplicity with tracking reliability, reduces noise in control signals, and aligns with the structural and dynamic requirements of SMS operating in microgravity environments.

Body Segment Motion Extraction and Analysis To analyze the biomechanical contributions of each anatomical segment during aerial righting, this study conducts a quantitative analysis of the angular motions of the body, tail, and limbs by transforming 2D motion data from image frames into 3D motion in the real world. That is, one evaluates segmental motions, such as (i) the orientation of each segment with respect to the inertial frame and (ii) the relative orientation of the limbs relative to the body.

Motion of Each Body Segment with respect to the Inertial Frame In the first stage, motions of all segments, including the body, tail, and limbs, are extracted with respect to the inertial frame. The 3D positions of anatomical landmarks (or keypoints), reconstructed from synchronized multi-camera video, are used to define rigid body segments as shown in Figure 5. Each segment is assigned a local coordinate frame, fixed on the respective body segment, constructed from anatomically meaningful keypoints.

For the main body, the x -axis unit vector ($\hat{\mathbf{x}}_b$) of the body-fixed reference frame is primarily defined as the normalized vector from the vent (keypoint 21) to the neck (keypoint 1). The temporary y -axis unit vector ($\hat{\mathbf{y}}_{b_{\text{temp}}}$), which generates the x - y plane, is formed using the vector from the right shoulder (keypoint 12) to the left shoulder (keypoint 13). After defining the z -axis unit vector ($\hat{\mathbf{z}}_b$) as the vector perpendicular to the x - y plane ($\hat{\mathbf{z}}_b = \hat{\mathbf{x}}_b \times \hat{\mathbf{y}}_{b_{\text{temp}}}$), the y -axis unit vector ($\hat{\mathbf{y}}_b$) is then determined using the right-hand rule. Based on these unit vectors, the direction cosine matrix (DCM) representing the rotation of the body reference frame with respect to the inertial frame is defined as:

$$C_{BN} = \begin{bmatrix} \hat{\mathbf{x}}_b^T \\ \hat{\mathbf{y}}_b^T \\ \hat{\mathbf{z}}_b^T \end{bmatrix}. \quad (3)$$

Similarly, the tail reference frame is defined using the tail tip (keypoint 23) and vent (keypoint 21) for the x -axis unit vector ($\hat{\mathbf{x}}_t$) and the hip joints (keypoints from 20 to 19) for the temporary y -axis unit vector ($\hat{\mathbf{y}}_{t_{\text{temp}}}$). Thus, the DCM for the tail motion (C_{TN}) is obtained following the same procedure as for the body-fixed reference frame.

For limb segments, local reference frames are primarily constructed using the leg-to-body vector as the y -axis: from the wrist (keypoints 8 (front) and 15 (hind)) to the shoulder (keypoint 12 (front)) and hip (keypoint 19 (hind)) for right legs, and from the shoulder (keypoint 13 (front)) and hip (keypoint 20 (hind)) to the wrist (keypoint 9 (front) and 16 (hind)) for the left legs. Note that the y -axis unit vector is expressed as $\hat{\mathbf{y}}_{l_i}$, where the subscript l_i represents left front, left hind, right front, and right hind legs, respectively.

Next, the z -axis unit vector ($\hat{\mathbf{z}}_{l_i}$) for each leg is defined as a vector that is orthogonal to the x - y plane produced by $\hat{\mathbf{y}}_{l_i}$ and the x -axis of the inertial frame. Then, the x -axis unit vector is determined as $\hat{\mathbf{x}}_{l_i} = \hat{\mathbf{y}}_{l_i} \times \hat{\mathbf{z}}_{l_i}$. Finally, the DCM for the motion of each leg with respect to the inertial frame ($C_{L_i N}$) is derived, similar to Eq. (3).



Figure 6: Sequences of Righting Reflex Motions (Top: side view, Bottom: front view)

While Figure 6 illustrates the primary sequences of the lizard’s righting reflex motions obtained from the free-fall video, Figure 7 shows the time-aligned attitude trajectories of the lizard’s body segments, which include the entire motion trajectory of the experimental video. To concentrate on the righting reflex of the lizard, the motion data for the specific time duration between 1,490 and 1,640 ms, highlighted in red in Figure 7a, is displayed on the right side of Figure 7. Note that the attitude information is represented by the 3-2-1 set of the Euler angles, which are converted from the DCMs of each body segment.

Since the direction from the vent to the neck aligns with the body’s roll direction, the primary motion changes in the body and tail during righting are observed along the roll axis, indicating aerial righting due to the transferred momentum from the tail rotation. Additionally, the extracted angular motions of each leg, particularly along the roll axis, shown in Figures 7c– 7f, follow a similar trend to the body’s roll motion, with increasing angles.

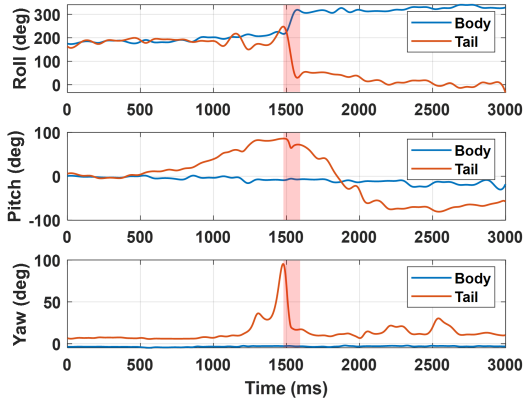
However, the roll angle at 1,640 ms in Figure 7b is less than 360 deg, which suggests that the body has not completed a full rotation, despite the righting sequence in Figure 5 showing a full rotation. While the primary righting reflex is achieved between 1,490 and 1,640 ms, additional body posture adjustments are observed after righting, as shown in Figure 7a. Furthermore, the video’s low-quality images in each frame may cause such a discrepancy, reducing accuracy. To address this, our research group is currently building a test environment for the lizards’ righting reflex using multiple high-speed cameras with different views, ensuring high-quality video capture for improved motion extraction accuracy.

Relative Leg Motion with respect to the Body As illustrated, the motion changes in each leg are also observed. Since the legs are connected to the body, it is required to explore the relative motion of the legs with respect to the body to analyze the impact of leg motion on the righting reflex.

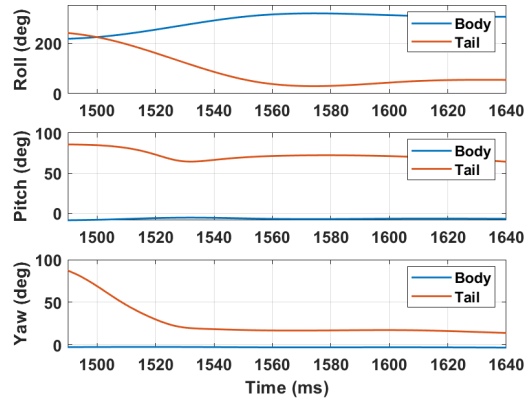
The relative rotation of each leg with respect to the body, defined as C_{L_iB} (L_i represents left front, left hind, right front, and right hind legs), is obtained by the successive rotations from the body to each leg, defined as

$$C_{L_iB} = C_{L_iN} C_{BN}^T. \quad (4)$$

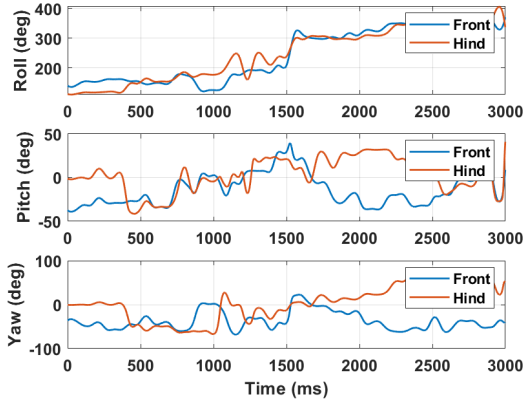
Figure 8 illustrates the relative angular trajectories of each leg relative to the body. One can



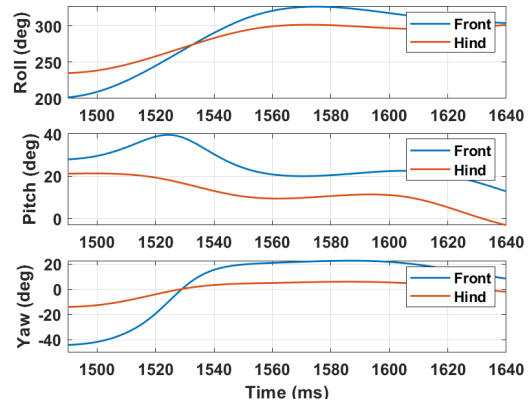
(a) Body and Tail (Entire Video)



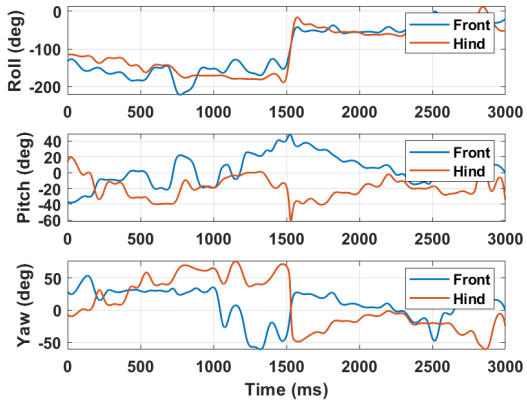
(b) Body and Tail (During Righting)



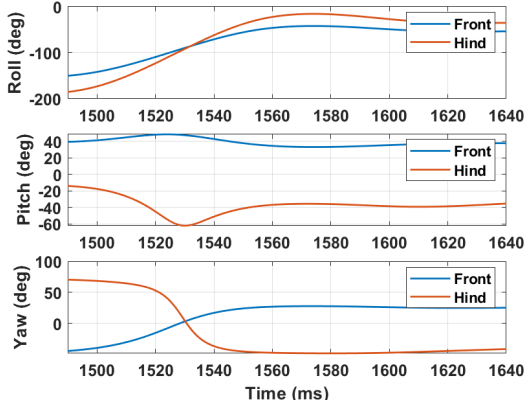
(c) Left Legs (Entire Video)



(d) Left Legs (During Righting)

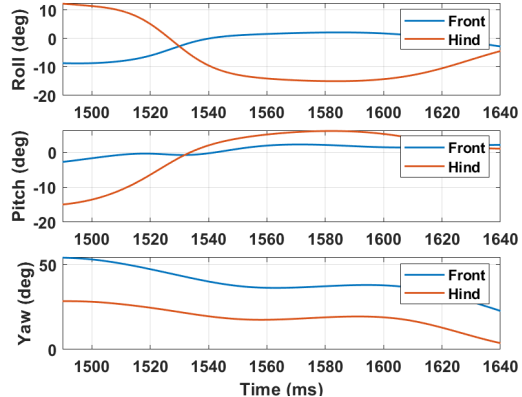


(e) Right Legs (Entire Video)

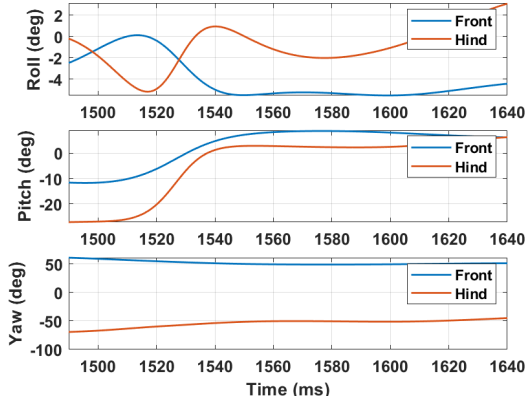


(f) Right Legs (During Righting)

Figure 7: Body Segment Motion with respect to the Inertial Frame



(a) Left Legs



(b) Right Legs

Figure 8: Legs' Relative Motion with respect to the Body During Righting

observe that the relative rolling motion changes, which is the primary motion during the righting reflex, remain small, around the zero angle, approximately within ± 15 deg. These findings suggest that the tail provides the dominant control for body posture stabilization during mid-air righting maneuvers, while the legs function as passive stabilizers, contributing negligibly to body motion.

This insight could inform the design of an energy-efficient SMS operational strategy, where leg actuation is reflected in the operation of the base spacecraft's attitude control actuators, which may help aid and/or correct the minor base motion changes, improving overall performance.

Integration and Control Evaluation in SMS (In progress)

The tasks in this step include analyzing the objectives and weighting factors for the optimization framework (defined in the first step) using the extracted motion trajectories. Then, these trajectories are leveraged as reference trajectories for the SMS, allowing the influence of different weights to be analyzed by observing the SMS's behaviors. However, due to the limited lizard's motion data available, the current work focuses primarily on implementing the extracted motion trajectory into the SMS.

Lizard's Body and Tail Motion Trajectory Analysis During Righting Given the similarities between the lizards and SMSs, the lizard's tail motion is primarily utilized as the reference input trajectory for the SMS. To confirm that the lizard's motion is applicable to SMSs, the orientation and rate along the roll axis, which is the primary axis for the righting reflex, are computed.

Note that the rate information is computed based on numerical differentiation using the orientation data. The entire maneuver occurs within a span of 150 ms, which results in a very high rotation rate of approximately 2,000 – 4,000 deg/s. Since such rapid movement is impractical for SMSs, the given trajectories (spanning 150 ms) are scaled to those with 225 s, which is more suitable for implementation on SMSs. It is important to note that the scaled time is based on the operational speed of the ETS-VII's robotic arm, which operates at approximately within 5 deg/s.²⁵

Using the scaled trajectory, the relative tail rotation with respect to the body is selected as the reference joint trajectory for the robotic arm of the SMS, as displayed in Figure 9. This is because the joint motion of the SMS is typically described with respect to the spacecraft base frame. The

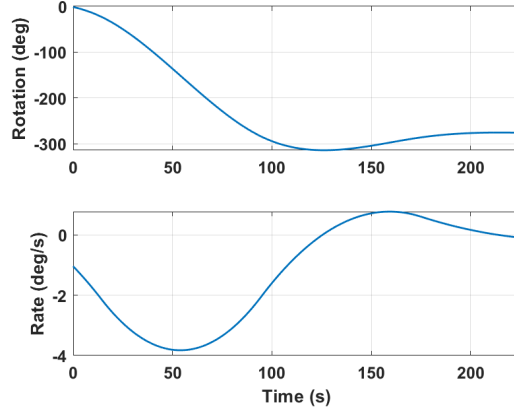


Figure 9: Scaled Relative Tail Motion with respect to the Body

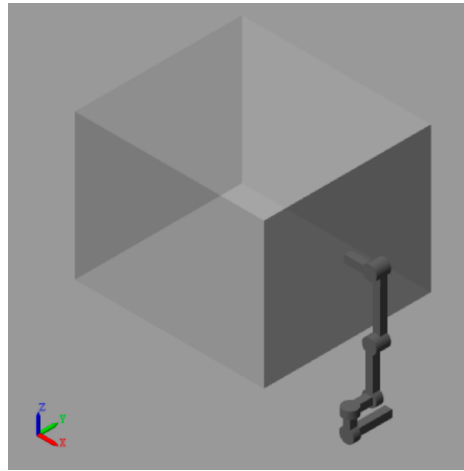


Figure 10: Simplified SMS Model Based on ETS-VII Specifications

characteristic information of this step response, assuming it reaches steady-state at 225 s, is summarized as follows: a rise time of 64.5 s, settling time of 169.5 s (within 5 % of the final value), and overshoot of 13.85 %. This motion trajectory, with these characteristics, will be implemented into the SMS as a reference trajectory for the first joint of the robotic arm.

Trajectory Implementation to SMS To implement the lizard’s motion trajectory into SMSs, this work considers an actual SMS model, ETS-VII, which has been tested in space. Based on the available specifications,¹ a simplified SMS model is built as illustrated in Figure 10. It is worth noting that the mass, inertia, and dimensions are identical to ETS-VII’s specifications, while the location of the robotic arm’s first link has been modified to align the first link’s rotation axis with the roll axis, similar to the alignment of the lizard frames in the motion extraction step. Moreover, the initial roll orientation of the base and first joint is set to around 180 deg to observe a motion trajectory similar to that of the lizard.

With this setting, the relative tail motion trajectory in Figure 9 is applied to the first joint, and the resultant SMS behavior is illustrated in Figure 11. Although the arm’s joint trajectory trend mirrors the relative tail trajectory, small motion changes in the base (orientation: less than 10 deg, rate:

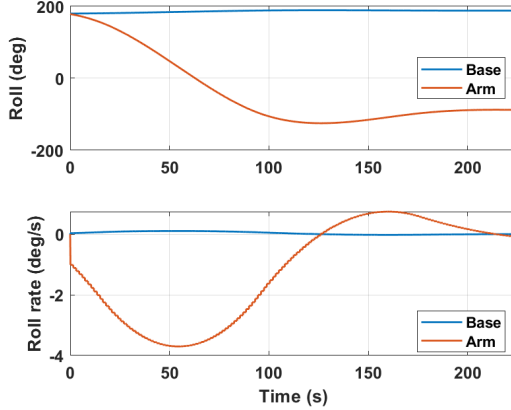


Figure 11: Lizard’s Scaled Trajectory-Implemented SMS Motion

less than 0.15 deg/s) are observed. This is expected because the base inertia is much greater than that of the robotic arm. In fact, if the base’s roll axis inertia is reduced by approximately 1/20, the SMS’s roll axis motion can be made to closely resemble the lizard’s roll motion trajectory shown in Figure 7b.

The different motion behaviors when implementing the lizard trajectory into the SMS are primarily due to the differences in inertia ratios between the lizard and SMS, as listed in Table 6, although they share a similar mass ratio. The inertia associated with the tail (or arm), which drives the body (or base) movement, is influenced by mass distribution, especially for the center of mass (CM) location. While the length ratio is not explicitly included in this comparison, it is implicitly captured in the CM calculation.

As indicated in the table, reducing the SMS’s roll axis inertia by 1/20 brings its inertia ratio closer to that of the lizard. This suggests that the mass and inertia ratio, considering mass distribution, are the dominant factors that contribute to the body rotation during righting.

As shown, direct implementation of the lizard’s motion into the SMS is possible, but impractical due to discrepancies, such as the inertia ratio, as well as the differing objectives behind the motion changes. However, it is still too early stage to conclude this analysis, as this work considers only one case of the lizard’s motion due to a lack of experimental data. Therefore, further work is required to analyze not only the lizard’s objectives and the combinations of the weighting factors but also to understand their behavior trends along with the step response characteristics. Additionally, analyzing relationships or correlations among the response characteristics, the mass and inertia ratios, and the relative importance of the objectives introduced in Eq. (1) is needed for a more in-depth analysis.

To remedy this, our research group is currently setting up an experimental environment for the lizard’s righting reflex tests, which will allow for the acquisition of more lizard motion data during righting using multiple high-speed cameras. Once these experimental data are obtained and analyzed, this step will be validated.

Table 6: Mass and Inertia Ratio Comparison

Parameter	Lizard ¹¹	SMS (ETS-VII) ¹
Mass ratio (tail / body or arm / base)	0.1	0.055
Body or base mass (kg)	2.9×10^{-3} kg	2550 kg
Tail or arm mass (kg)	0.29×10^{-3} kg	140.4 kg
Inertia ratio (tail / body or arm / base)	0.8	0.056*
Body or base inertia (kg-m ²)	6.6×10^{-8}	6200 (roll axis)
Tail or arm inertia governed by CM** (kg-m ²)	5.29×10^{-8}	360

* When the base inertia is adjusted by 1/20, the inertia ratio is changed to 0.86, resulting in similar behaviors.

** The effective inertia affecting the body or base rotation is the one governed by the CM (center of mass) location.

CONCLUSIONS

This work presents a biologically inspired approach for space manipulator system (SMS) operations by translating lizard righting reflex behaviors into reference motion trajectories for SMSs. Through a structured analysis, this study establishes morphological, behavioral, and environmental analogies demonstrating the feasibility of leveraging evolved motion patterns of lizards for SMS operations. Moreover, using a computer vision pipeline, air-righting motion trajectories are extracted and analyzed, confirming that tail dynamics primarily drive reorientation for body posture stabilization while limb motions contribute to secondary stabilization or minor motion change. The extracted lizard’s motion trajectory is then implemented into the SMS, observing its feasibility and identifying discrepancies between the lizards and SMSs. These insights support the formulation of interpretable multi-objective optimization problem settings balancing stability, safety, and efficiency. Limitations include the small dataset and the need to appropriately rescale motion profiles for practical SMS implementation. Future work will acquire lizard experimental motion data to validate the final step. Overall, this study provides the basis for incorporating biological principles into robust and interpretable control architectures for space robotics.

ACKNOWLEDGEMENT

This material is based upon work supported by the Air Force Office of Scientific Research under award number FA9550-24-1-0600.

REFERENCES

- [1] K. Yoshida, “Engineering Test Satellite VII Flight Experiments for Space Robot Dynamics and Control: Theories on Laboratory Test Beds Ten Years Ago, Now in Orbit,” *The International Journal of Robotics Research*, Vol. 22, No. 5, 2003, pp. 321–335, 10.1177/0278364903022005003.
- [2] J. Shoemaker, M. Wright, and S. Sivapiragasam, “Orbital Express Space Operations Architecture Program,” *17th Annual AIAA/USU Conference on Small Satellites*, Defense Advanced Research Projects Agency (DARPA), 2003, pp. 1–8.
- [3] G. S. Rodrigues and T. F. P. A. T. Pazelli, “Dynamic Modeling and Control Optimization of Free-Floating Dual-Arm Space Robots in Task Space,” *2021 Latin American Robotics Symposium (LARS), 2021 Brazilian Symposium on Robotics (SBR), and 2021 Workshop on Robotics in Education (WRE)*, 2021, pp. 168–173, 10.1109/LARS/SBR/WRE54079.2021.9605469.
- [4] D. Qiao, “Motion Planning Optimization Of Trajectory Path Of Space Manipulators,” *International Journal of Metrology and Quality Engineering*, Vol. 10, 2019, p. 11.
- [5] A. Tringali and S. Cocuzza, “Finite-Horizon Kinetic Energy Optimization of a Redundant Space Manipulator,” *Applied Sciences*, Vol. 11, No. 5, 2021, 10.3390/app11052346.

- [6] J. Blaise and M. C. F. Bazzocchi, "Space Manipulator Collision Avoidance Using a Deep Reinforcement Learning Control," *Aerospace*, Vol. 10, No. 9, 2023, 10.3390/aerospace10090778.
- [7] L. Li, Y. Xie, Y. Wang, and A. Chen, "Reinforcement Learning of Space Robotic Manipulation with Multiple Safety Constraints," *2022 41st Chinese Control Conference (CCC)*, 2022, pp. 7376–7382, 10.23919/CCC55666.2022.9902690.
- [8] L. Longo, M. Brcic, F. Cabitz, J. Choi, R. Confalonieri, J. D. Ser, R. Guidotti, Y. Hayashi, F. Herrera, A. Holzinger, R. Jiang, H. Khosravi, F. Lecue, G. Malgieri, A. Páez, W. Samek, J. Schneider, T. Speith, and S. Stumpf, "Explainable Artificial Intelligence (XAI) 2.0: A manifesto of open challenges and interdisciplinary research directions," *Information Fusion*, Vol. 106, 2024, p. 102301, <https://doi.org/10.1016/j.inffus.2024.102301>.
- [9] T. R. Kane and M. P. Scher, "A Dynamical Explanation of the Falling Cat Phenomenon," *International Journal of Solids and Structures*, Vol. 5, No. 7, 1969, pp. 663–666.
- [10] T. Fukushima, R. Siddall, F. Schwab, S. L. D. Toussaint, G. Byrnes, J. A. Nyakatura, and A. Jusufi, "Inertial Tail Effects during Righting of Squirrels in Unexpected Falls: From Behavior to Robotics," *Integrative and Comparative Biology*, Vol. 61, 04 2021, pp. 589–602, 10.1093/icb/icab023.
- [11] A. Jusufi, D. I. Goldman, S. Revzen, and R. J. Full, "Active Tails Enhance Arboreal Acrobatics in Geckos," *Proceedings of the National Academy of Sciences*, Vol. 105, No. 11, 2008, pp. 4215–4219.
- [12] A. Jusufi, Y. Zeng, R. J. Full, and R. Dudley, "Aerial Righting Reflexes in Flightless Animals," *Integrative and Comparative Biology*, Vol. 51, 09 2011, pp. 937–943, 10.1093/icb/icr114.
- [13] A. Jusufi and R. J. Full, "A Lizard-Inspired Active Tail Enables Rapid Maneuvers and Dynamic Stabilization in a Terrestrial Robot," *Bioinspiration & Biomimetics*, Vol. 6, No. 2, 2011, p. 026007.
- [14] E. Chang-Siu, T. Libby, M. Tomizuka, and R. J. Full, "A Lizard-Inspired Active Tail Enables Rapid Maneuvers and Dynamic Stabilization in a Terrestrial Robot," *Proceedings of the IEEE International Conference on Intelligent Robots and Systems*, 2011, pp. 1887–1893.
- [15] L. A. Dugatkin, *Principles Of Animal Behavior*. University of Chicago Press, 2020.
- [16] D. J. Irschick and B. C. Jayne, "Comparative three-dimensional kinematics of the hindlimb for high-speed bipedal and quadrupedal locomotion of lizards," *Journal of Experimental Biology*, Vol. 202, 05 1999, pp. 1047–1065, 10.1242/jeb.202.9.1047.
- [17] A. Antonello, A. Valverde, and P. Tsotras, "Dynamics and Control of Spacecraft Manipulators with Thrusters and Momentum Exchange Devices," *Journal of Guidance, Control, and Dynamics*, Vol. 42, No. 1, 2019, pp. 15–29, 10.2514/1.G003601.
- [18] V. Barabanov, V. Gulimova, R. Berdiev, and S. Saveliev, "Object play in thick-toed geckos during a space experiment," *Journal of Ethology*, Vol. 33, 2015, pp. 109–115, 10.1007/s10164-015-0426-8.
- [19] V. Gulimova, A. Proshchchina, A. Kharlamova, Y. Krivova, V. Barabanov, R. Berdiev, V. Asadchikov, A. Buzmakov, D. Zolotov, and S. Saveliev, "Reptiles in Space Missions: Results and Perspectives," *International Journal of Molecular Sciences*, Vol. 20, No. 12, 2019, p. 3019, 10.3390/ijms20123019.
- [20] A. Vera and D. Kim, "Kinematic Adaptation in Space Robotics Inspired by Animal Righting Reflexes," *2025 Regional Student Conferences (In press)*, 2025.
- [21] A. Kirillov, E. Mintun, N. Ravi, H. Mao, C. Rolland, and L. e. a. Gustafson, "Segment Anything," *arXiv preprint*, Vol. arXiv:2304.02643, 2023.
- [22] Y. Xu, J. Zhang, Q. Zhang, and D. Tao, "ViTPose++: Vision Transformer for Generic Body Pose Estimation," *IEEE Transactions on Pattern Analysis & Machine Intelligence*, Vol. 46, Feb. 2024, pp. 1212–1230, 10.1109/TPAMI.2023.3330016.
- [23] N. Karaev, I. Rocco, B. Graham, N. Neverova, A. Vedaldi, and C. Rupprecht, "CoTracker: It is Better to Track Together," *arXiv preprint*, Vol. arXiv:2307.07635, 2023.
- [24] A. Jusufi, D. T. Kawano, T. Libby, and R. J. Full, "Righting and turning in mid-air using appendage inertia: reptile tails, analytical models and bio-inspired robots," *Bioinspiration & Biomimetics*, Vol. 5, nov 2010, p. 045001, 10.1088/1748-3182/5/4/045001.
- [25] S. Abiko and K. Yoshida, "Post flight analysis of ETS-VII space robotic experiments," *6th International Symposium on Artificial Intelligence and Robotics and Automation in Space, St-Hubert, Quebec, Canada*, 2001.